Progress In Electromagnetics Research, PIER 100, 327–349, 2010

INVESTIGATION INTO TIME- AND FREQUENCY-DOMAIN EMI-INDUCED NOISE IN BISTABLE MULTIVIBRATOR

H.-C. Tsai

Department of Electronic Engineering
Cheng-Shiu University
No. 840, Chengcing Rd., Neausong Township, Kaohsiung County
Taiwan 83305, R.O.C.

Abstract—Electromagnetic interference (EMI) has a negative effect upon the performance of circuit communication systems. The present study considers the case of EMI induced in a conducting wire, and derives equations to establish the effect of the EMI on a bistable multivibrator. The validity of the equations is verified experimentally. The results indicate that the degree of influence of the EMI on the bistable oscillator depends on the interference power, the interference frequency, the induced power, the output resistance of the circuit, and the parasitic capacitance. Moreover, it is shown that the harmonic noise increases with an increasing interference amplitude and frequency. The theoretical results are found to be in good agreement with the experimental data.

1. INTRODUCTION

Since digital circuits can only exist in one of two different discrete binary states, i.e., "on and off" or "high and low", they are more reliable than their analogue counterparts, whose characteristics and states are continuous. As a result, digital IC devices are widely used in many fields throughout engineering and industry. In developing IC circuits, the sensitivity of the device performance to external factors such as the component values, component aging, the ambient temperature, interference signals, EMI and shielding has attracted particular attention. With the prevalence of Radio Frequency (RF) applications [1, 2] nowadays, such as TVs and radios, amateur radio,

Corresponding author: H.-C. Tsai (hctsai@csu.edu.tw).

wireless "walkie-talkies", cell phones, wireless remote controllers, Blue Tooth communication systems [3, 4], and so on, the environment is rapidly becoming saturated with electromagnetic waves. Some of these electromagnetic waves, termed as "signals", are useful and necessary in that they fulfill a specific design purpose. However, others are undesirable since they interfere with the performance of other electrical or electronic devices. For example, it is well known that a cell phone used in close proximity to a computer may cause a distortion of the image on the screen or a static blast from the speakers. Similarly, cell phones may disrupt the delicate flight instrumentation onboard an aircraft and are therefore banned in flight. Finally, in a communications/broadcasting context, interference may be manifested in the form of "cross talk", a phenomenon in which the conversations of others are detected when speaking over the cell phone, or may result in the reception of two different radio stations at the same frequency. Whilst in some cases, the effects of EMI are no more than a minor irritant (e.g., the screen distortion caused by the use of a wireless emitting device near a TV), in others, they may be potentially lethal (e.g., the use of a cell phone onboard an aircraft). As a result, it is essential that the effects of EMI on common electronic components are thoroughly understood [5–19]. Accordingly, the present study considers the EMI response of a bistable multivibrator, a component with wide-ranging applications in the electronics field, including Ref. [20–22]. In a normal indoor environment, the intensity of the low frequency electromagnetic waves is greater than that of the high frequency waves, i.e., $0.03\,\mu T$ and $0.0067\,\mu T$, respectively (as measured by the current authors using CA40/43 instrumentation (Chauvin Arnoux, France)). Therefore, in analyzing the effects of EMI on the bistable multivibrator, the present analyses focus specifically on the effects of low frequency EMI.

2. EXPERIMENTAL SETUP

Figure 1 illustrates the experimental setup used in this study to measure the interference noise spectrum induced in the bistable multivibrator. The arrangement has the advantage that both the amplitude and the frequency of the EMI noise can be easily controlled. As shown, the experimental system was shielded within a metal case to suppress the effects of external noise, and the amplifier and current source were both battery operated. In the experiments, EMI with a frequency ranging from $200 \sim 900\,Hz$ and an amplitude between $0.2\,V$ and $0.9\,V$ was induced in a conducting wire (CW) positioned in the air gap of a ferromagnetic toroid wrapped with a current-carrying

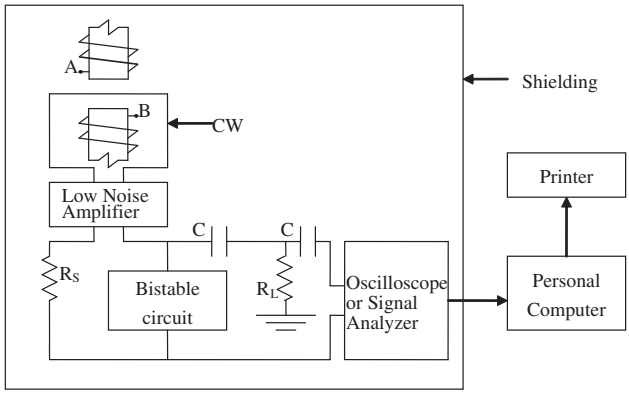

Figure 1. Experimental setup for noise measurement in bistable multivibrator.

coil, where CW is a circular wire with aluminum alloy material, the diameter is 0.001 m. The EMI interference was detected initially as radiated noise, amplified by a 73.98 dB low-noise pre-amplifier such that it could be detected using an oscilloscope, and then coupled in series with the bistable multivibrator in the form of conducted noise. The EMI signals were transmitted to the oscilloscope via a circuit coupling and were then passed to a spectrum analyzer (model HP E4440A) controlled by a PC via an IEEE-488 bus in order to obtain the time domain and frequency spectrum plots of the interference signals.

3. THEORETICAL ANALYSIS

Multivibrators are two-state, digital circuits which employ positive feed-back during state changes. Three different classes of multivibrator exist, namely bistable, monostable, and astable. The bistable multivibrator, also known as a flip-flop, latch or binary circuit, is characterized by two stable states, which persist indefinitely unless deliberately changed. Of all the multivibrators, the bistable multivibrator is one of the most commonly used (typically for applications such as single bit information storage), and is therefore chosen for analysis purposes in the present study.

3.1. Basic Parameters of Bistable Multivibrator

Figure 2 presents the basic circuit of a bistable multivibrator. Let the logical output state of the multivibrator be denoted as Q. When $Q = 1$, the inverter has a complementary logical output, i.e., $\overline{Q}$=0. This state

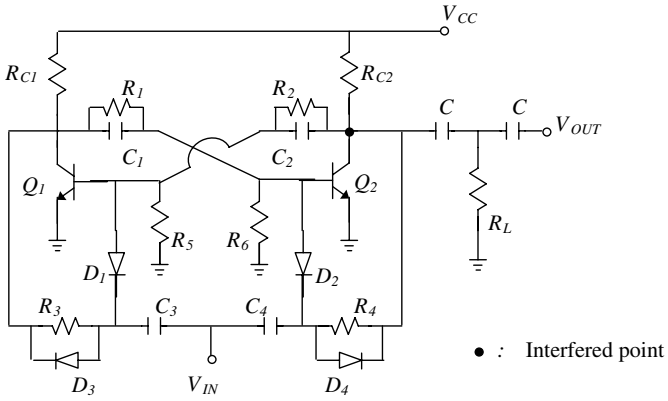

Figure 2. Bistable multivibrator circuit.

persists until an excitation signal is applied, at which point it flip-flops to the complementary value. This new state is then maintained until a further excitation signal is applied, and so on. As shown in Fig. 2, the multivibrator circuit is symmetrical, i.e., $R_{C1} = R_{C2}$, $C_1 = C_2$, $R_1 = R_2$, $R_3 = R_4$, $R_5 = R_6$, and $C_3 = C_4$, Q_1 and Q_2 are the same type, but which is impossible to have the same characteristics. Furthermore, transistors Q_1 and Q_2 are of same type, but have different characteristics such that when one is "on", the other is "off".

3.1.1. Circuit Design

Assume that when the power is initially turned on, Q_1 is "on" and Q_2 is "off". Assume also that $V_{CE1(sat)} = 0.2^V$ and $R_{C1} = R_{C2} = 1^K$.

From the circuit, it can be shown that

$$I_{C1(sat)} = \frac{V_{CC} - 0.2^V}{R_{C1}} = \frac{1.4 - 0.2}{1^K} = 1.2\,\text{mA} \tag{1}$$

Check

$$\beta I_{B1} > I_{C1(sat)} \tag{2}$$

$$I_{B1(sat\cdot\min)} \geq \frac{I_{C1(sat)}}{\beta} = \frac{1.2\,\text{mA}}{157} = 7.64\,\mu\text{A} \tag{3}$$

Select $V_{CE2(off)} = 1.05^V$

$$I_{C2(off)} = \frac{V_{CC} - V_{CE2(off)}}{R_{C2}} = \frac{1.4 - 1.05}{1^K} = 0.35\,\text{mA} \tag{4}$$

Obtain

$$R_2 = \frac{V_{CE2(off)} - V_{BE1(sat)}}{I_{C2(off)}} = \frac{1.05^V - 0.7^V}{0.35\,\text{mA}} = 1^K \tag{5}$$

Select $R_5 = 2.2^K$

$$I_{R5} = \frac{V_{BE1}}{R_5} = \frac{0.7}{2.2^K} = 0.318\,\text{mA} \tag{6}$$

Obtain

$$\begin{aligned} I_{B1} &= I_{C2(off)} - I_{R5} = 0.35\,\text{mA} - 0.318\,\text{mA} \\ &= 32\,\mu\text{A} > I_{B1(sat\cdot\min)} = 7.64\,\mu\text{A} \end{aligned} \tag{7}$$

From Kirchhoff's voltage law, it follows that

$$R_{C1} \ll R_1 + R_6, \quad R_{C2} \ll R_2 + R_5 \tag{8}$$

Select

$$V_{CE2(off)} = 1.05^V,$$

Implies

$$V_{RC2} = 1.4^V - 1.05^V = 0.35^V$$

Check

$$V_{RC2} = 1.4^V \frac{1^K}{1^K + 1^K + 2.2^K} = 0.33^V \cong 0.35^V$$

Differential Circuit:
Select

$$R_3 = 12R_{C1} = 12^K = R_4, \quad f = 20^K, \quad T = 50\,\mu\text{s},$$

Take

$$C_3 = C_4 = 0.001\,\mu\text{f}$$

3.2. Electromagnetic Interference

In the present study, the interference source has the form of a current-carrying coil wound on a ferromagnetic toroid with an air gap. When a current is passed through the coil, an EMI voltage of magnitude V_{eff} is induced in a conducting wire (CW) positioned within the air gap. The magnetic field density and flux density in the air gap are given respectively by [23]

$$H_g = \frac{\mu N I_0}{\mu_0 (2\pi r_0 - l_g) + \mu l_g} \tag{9}$$

$$P_{rB} = \frac{1}{2}\int \mu_0 H_g^2 dv = \frac{1}{2}\int H_g B_g dv \tag{10}$$

where μ_0 is the permeability of free space, μ is the permeability of the ferromagnetic material, I_0 is the current within the coil, r_0 is the mean radius of the toroid, and l_g is the width of the air gap. The value of P_{rB} represents the average energy per second of the interference on the CW, and can be calculated from Eq. (10) or measured directly.

In general, any periodic signal can be represented by the following complex Fourier series:

$$V(t) = \sum_{n=-\infty}^{\infty} C_n e^{jn\omega t} = C_0 + \sum_{n=1}^{\infty} 2\left|C_n\right| \cos\left(n\omega t + \angle C_n\right) \tag{11}$$

where

$$C_n = \frac{1}{T}\int_{-\frac{T}{2}}^{\frac{T}{2}} V\left(t\right) e^{jn\omega t} dt \tag{12}$$

In the present experiments, the input signal of the ferromagnetic toroid has the form of a periodic square wave, as shown in Fig. 3. In this case, the following Fourier transform applies:

$$C_n = \frac{1}{T}\int_0^{t_0} V_0\left(t\right) e^{-jn\omega t} dt = \frac{V_0 t_0}{T} \frac{\sin\frac{1}{2}n\omega t_0}{\frac{1}{2}n\omega t_0} e^{-j\frac{1}{2}n\omega t_0} \tag{13}$$

and

$$K_n = \frac{V_0 t_0}{T} \frac{\sin\frac{1}{2}n\omega t_0}{\frac{1}{2}n\omega t_0} \tag{14}$$

$$\angle C_n = \frac{1}{2} n\omega t_0 \tag{15}$$

Substituting Eqs. (14) and (15) into Eq. (11) gives

$$V\left(t\right) = \frac{V_0}{2} + \sum_{n=1}^{\infty} K_n \cos\left(n\omega t_0 + \frac{n\pi}{2}\right), \text{ for } t_0 = \frac{T}{2} \tag{16}$$

Figure 4 shows the equivalent circuit of the ferromagnetic toroid. The following admittance can be obtained:

$$\begin{aligned} Y &= \frac{\left(R_\omega + jn\omega L\right) + \frac{1}{jn\omega C_\omega}}{\left(R_\omega + jn\omega L\right)\frac{1}{jn\omega C_\omega}} \\ &= \frac{1}{R_\omega^2 + n^2\omega^2 L^2}\left[R_\omega + j\left(n\omega R_\omega^2 C_\omega - n\omega L + n^3\omega^3 L^2 C_\omega\right)\right] = \left|Y\right|\angle\theta_1 \end{aligned} \tag{17}$$

$$I\left(jn\omega\right) = YV\left(t\right) = C_0 Y_0 + \sum_{n=1}^{\infty} 2K_n\left|Y\right| \cos\left(n\omega t + \angle C_n + \theta_1\right) \tag{18}$$

From Eq. (9), it can be shown that

$$\begin{aligned} V_{eff} &= -\frac{1}{dt}\int_s \vec{B}\cdot d\vec{s} = -\frac{1}{dt}\left[\frac{\mu_0\mu NI\left(jn\omega\right)}{\mu_0\left(2\pi r_0 - l_g\right)+\mu l_g}\cdot \Delta z d\right] \\ &= \frac{\mu_0\mu N\left(\Delta z d\right)}{\mu_0\left(2\pi r_0 - l_g\right)+\mu l_g}\sum_{n=1}^{\infty} 2K_n\left|Y\right| n\omega \sin\left(n\omega t + \angle C_n + \theta_1\right) \\ &= \sum_{n=1}^{\infty} 2KK_n\left|Y\right| n\omega \sin\left(n\omega t + \angle C_n + \theta_1\right) \qquad (19) \end{aligned}$$

$$K = \frac{\mu_0\mu N\Delta z d}{\mu_0\left(2\pi r_0 - l_g\right)+\mu l_g} \qquad (20)$$

Figure 5 shows the equivalent circuit of the experimental measurement system.

The V_{out} signal supplied to the oscilloscope and signal analyzer is given by

$$V_{out} = V_{eff}\frac{K_1}{R_S}\cdot\frac{K_3\angle\theta_3}{K_2\angle\theta_2}\cdot\frac{R_i}{K_4\angle\theta_4} \qquad (21)$$

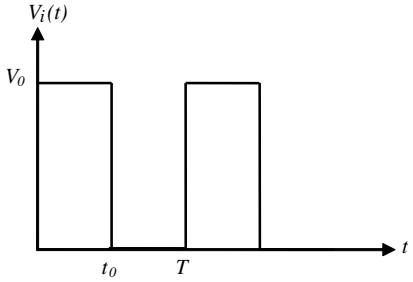

Figure 3. Experimental input signal of ferromagnetic toroid.

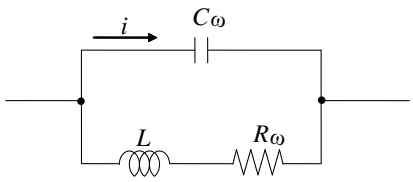

Figure 4. Equivalent circuit of ferromagnetic toroid.

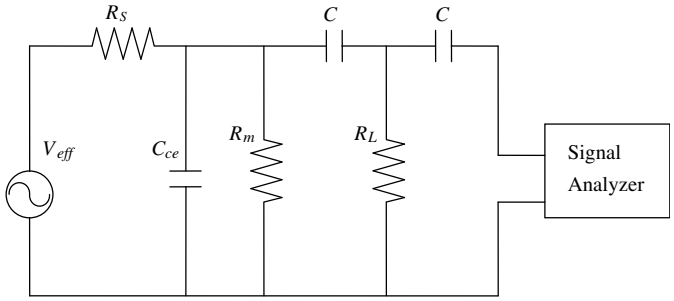

Figure 5. Equivalent circuit of experimental measurement system.

where $K_1 = R_S//R_m,\ R_m = 1/h_{oe}//R_{c2}//R_2//R_4$ for a small value of C_{ce}.

$$Q_2 = K_1 - j\frac{1}{\omega C} = K_2\angle\theta_2 \tag{22}$$

$$K_2 = \left[K_1^2 + \left(\frac{1}{\omega C}\right)^2\right]^{\frac{1}{2}} \quad \theta_2 = \tan^{-1}\frac{-\frac{1}{\omega C}}{K_1} \tag{23}$$

$$Q_3 = K_2\angle\theta_2//R_L = K_3\angle\theta_3 = a + bj \tag{24}$$

$$K_3 = \frac{1}{(K_1+R_2)^2 + \left(\frac{1}{\omega C}\right)^2} \left\{\left[K_1R_L(K_1+R_L) + \frac{R_2}{\omega^2C^2}\right]^2 + \left[\frac{K_1R_L}{\omega C} - (K_1+R_L)\frac{R_L}{\omega C}\right]^2\right\}^{1/2}$$

$$\theta_3 = \tan^{-1}\frac{\frac{K_1R_L}{\omega C} - (K_1+R_L)\frac{R_L}{\omega C}}{K_1R_L(K_1+R_L) + \frac{R_L}{\omega^2C^2}} \tag{25}$$

$$Q_4 = (R_S//R_m + X_C)//R_L + X_C + R_i = Q_3 + X_C + R_i$$

$$= a + R_i + j\left(b - \frac{1}{\omega C}\right) = K_4\angle\theta_4 \tag{26}$$

$$K_4 = \left[(a+R_i)^2 + \left(b - \frac{1}{\omega C}\right)^2\right]^{\frac{1}{2}} \tag{27}$$

$$\theta_4 = \tan^{-1}\frac{b - \frac{1}{\omega C}}{a + R_i} \tag{28}$$

From the above, it can be shown that

$$V_{out} = \sum_{n=1}^{\infty}\frac{2KK_n|Y|n\omega K_1K_3R_i\sin(n\omega t + \angle C_n + \theta_1 + \theta_3 - \theta_2 - \theta_4)}{R_sK_2K_4}$$

$$V_{out} = \sum_{n=1}^{\infty}\frac{C_3 2KK_n|Y|n\omega K_1K_3R_i}{R_sK_2K_4}\sin(n\omega t + \angle C_n + \theta_1 + \theta_3 - \theta_2 - \theta_4) \tag{29}$$

where the constant C_3 is the effective inducted coefficient. Eq. (29) shows that the magnitude of the EMI-induced noise is governed by the pulse height, the output load, the parasitic capacitance, the interference frequency and the interference amplitude.

3.3. Noise Analysis

Conducting wires render IC circuits highly susceptible to the effects of electromagnetic interference and noise [24–29]. When a periodic

square wave is applied across points A and B in Fig. 1, the CW in the air gap of the ferromagnetic torroid induces a pulse voltage in the bistable multivibrator circuit, which in turn produces a response noise spectrum. Fig. 6 shows the typical response wave for a periodic pulse with a period T. The periodic pulse function can be analyzed by taking the discrete Fourier transformation of function S_n, where S_n is a function of A_1 and A_2 (i.e., the pulse heights), i.e.,

$$S_n = \frac{1}{T}\left[\int_{-T_0}^{0} -A_1 e^{-a(T_0+t)} e^{-j\omega nt} dt + \int_{0}^{T_0} A_2 e^{-at} e^{-j\omega nt} dt\right]$$
$$= \frac{1}{T}\frac{a - j\omega n}{a^2 + \omega^2 n^2}\left[E - jD\right] \tag{30}$$

where

$$E = A_1 e^{-aT_0} + A_2 - A_2 e^{-aT_0}\cos\omega nT_0 - A_1\cos\omega nT_0 \tag{31}$$
$$D = -A_2 e^{-aT_0}\sin\omega nT_0 + A_1\sin\omega nT_0 \tag{32}$$
$$S_n^2 = \frac{1}{T^2(a^2 + \omega^2 n^2)}\left[E^2 + D^2\right] \tag{33}$$

in which n is an integer, $\omega = 2\pi f = 2\pi/T$, a is the attenuation factor of the exponential function, and A_1 and A_2 are the amplitudes of the upper-half and lower-half periods of the EMI induced by the CW, respectively.

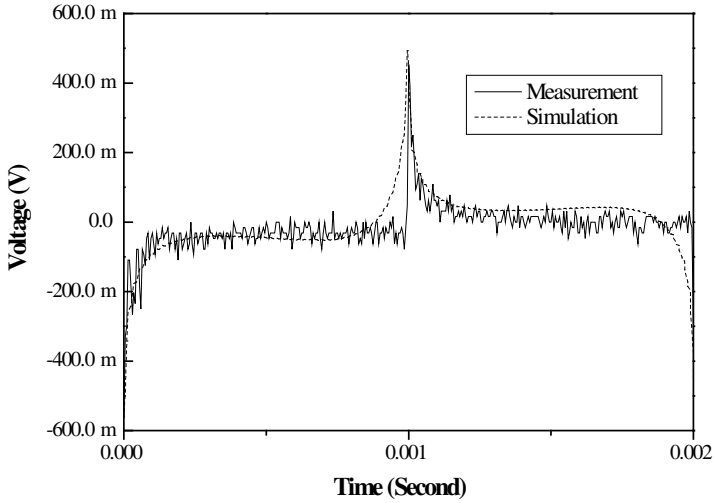

Figure 6. Experimental and simulation results for typical periodic pulse wave generated by periodic EMI signal with period T.

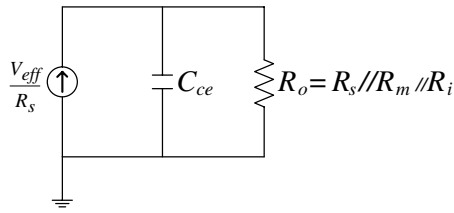

Figure 7. Simplified representation of EMI output port in Fig. 1.

The amplitude spectrum of the EMI current can be obtained by plotting S_n against discrete frequencies, i.e., ωn. The square of S_n has dimensions A^2 and corresponds to the current power spectrum $S_{i\lambda}(f_n)$ over $2T$ [30].

Figure 7 shows the Norton equivalent output circuit of the bistable multivibrator, where C_{ce} is the parasitic capacitance between the drain and the source. Let $V_{ce} = V_C$ and $C_{ce} = C$, then

$$i_n = i_C + i_0 = C\frac{d\Delta V_C}{dt} + \frac{\Delta V_C}{R_0} \Rightarrow \frac{d\Delta V_C}{dt} + \frac{\Delta V_C}{R_0 C} = \frac{i_n}{C} \tag{34}$$

where $R_0 = R_s//R_m//R_i$, and ΔV_c is the variation in the voltage across the capacitor.

Taking the Fourier series expansions of ΔV_c and i_λ gives

$$\frac{i_n}{C} = \frac{1}{C}\sum_{n=-\infty}^{\infty} \alpha_n \exp(j\omega_n t) \tag{35}$$

$$\frac{d(\Delta V_{cn})}{dt} + \frac{\Delta V_{cn}}{R_0 C} = \frac{1}{C}\alpha_n \exp(j\omega_n t) \tag{36}$$

From which it can be shown that

$$\Delta V_{cn} = \beta_n \exp(j\omega_n t) \tag{37}$$

where

$$\beta_n = \frac{\alpha_n R_0}{1 + j\omega_n R_0 C} \tag{38}$$

Therefore, the noise power spectrum, $S_{\Delta Vc}(f_n)$, of the bistable multivibrator induced by the EMI is given by

$$S_{\Delta Vc}(f_n) = 2T\overline{\beta_n \beta_n^*} \tag{39}$$

$$S_{\Delta Vc}(f_n) = S_{i\lambda}(f_n)\frac{R_0^2}{1 + (\omega_1 n R_0 C)^2} \tag{40}$$

where

$$S_{i\lambda}(f_n) = 2T\overline{\alpha_n \alpha_n^*} = 2TS_n^2 \tag{41}$$

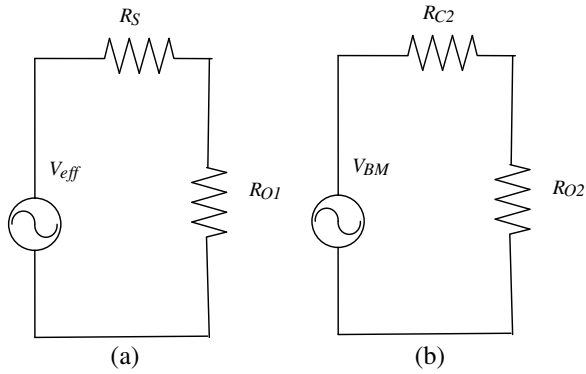

Figure 8. Output equivalent circuits of (a) EMI signal and (b) bistable multibibrator signal.

From Eqs. (5), (12) and (13), it can be shown that

$$S_{\Delta V_C}(f_n) = 2T\frac{R_0^2}{1+(\omega_1 n R_0 C)^2}\left[\frac{1}{T^2(a^2+\omega^2 n^2)}(E^2+D^2)\right] \quad (42)$$

The total noise power induced in the bistable multivibrator can be obtained by summing $S_{\Delta Vc}(f_n)$ over all possible integers, n. In identifying the relative magnitudes of the various harmonic components within the power spectrum, the present analysis first finds the value of A (the pulse height) from the measured power spectral intensity of the fundamental harmonic and then evaluates the power spectral intensities of the higher-order harmonics. Adopting this approach, the typical experimental response wave shown in Fig. 6 can be transformed into the noise spectrum shown in Fig. 9 and the value of the EMI then quantified directly.

3.4. Effects of Basic Bistable Multivibrator Frequency on Output Power

The basic output frequency of a bistable multivibrator has the form of a square wave. Generally speaking, the effects of the basic output frequency on the noise power spectrum of the multivibrator can be mitigated using an impedance-matching method. Fig. 8(a) shows the output equivalent circuit of the EMI signal supplied to the oscilloscope or signal analyzer, where $R_{O1} = 1/h_{oe}//R_{C2}//R_2//R_4//R_L//R_i = 45.21\,\Omega$. Meanwhile, Fig. 8(b) shows the equivalent circuit of the bistable multivibrator square wave output signal, where $R_{O2} = 1/h_{oe}//R_S//R_2//R_4//R_L//R_i = 24.31\,\Omega$. The output powers of the

EMI and multivibrator signals can be obtained respectively as

$$P_{EMI} = \left(\frac{V_{eff}}{50 + 45.21}\right)^2 45.21 = 0.005(V_{eff})^2 \quad (43)$$

$$P_{BM} = \left(\frac{V_{BM}}{1^k + 24.31}\right)^2 24.31 = 2.32 \times 10^{-5}(V_{BM})^2 \quad (44)$$

Here, $P_{BM}/P_{EMI} = 0.0046$. In other words, the output power of the bistable multivibrator is negligible compared to that of the EMI induced signal and can therefore be neglected.

4. RESULTS AND DISCUSSION

Figure 6 presents the experimental and simulation results for the typical periodic pulse function generated by a periodic EMI signal with a period T. Note that in obtaining the simulation results using Eq. (29), the following parameter settings are assumed: $V_0 = 0.56\,\mathrm{V}$ (at time $t = 0$), $V_0 = 0.45\,\mathrm{V}$ (at time $t = T/2$), $\mu_0 = 4\pi E - 7\,\mathrm{H/m}$, $\mu_r = 4000$, $N = 500$, $F = 500\,\mathrm{Hz}$, $R_\omega = 0.52\,\Omega$, $r_0 = 0.09\,\mathrm{m}$, $l_g = 0.005\,\mathrm{m}$, $C_\omega = 6.558E - 10\,\mathrm{F}$, $1/h_{oe} = 30\,\mathrm{k}\Omega$, $R_{c1} = R_{c2} = 1\,\mathrm{k}\Omega$, $R_1 = R_2 = 1\,\mathrm{k}\Omega$, $R_3 = R_4 = 12\,\mathrm{k}\Omega$, $C = 100E - 6\,\mathrm{F}$, $\Delta z = 0.01\,\mathrm{m}$, $d = 0.001\,\mathrm{m}$, $R_s = 50\,\Omega$, $C_3 = 0.081$, $X_C = 1/(2\pi f C)$, $R_L = 220\,\mathrm{k}\Omega$, $L = 1E - 4\,\mathrm{H}$, $\omega = 2\pi f$ and $R_i = 50\,\Omega$. Fig. 6 confirms that a good agreement exists between the simulated pulse function and the experimental function. In the experimental setup shown in Fig. 1, $C_{ce} = 12.77E - 8\,\mathrm{F}$, $R_L = 220\,\mathrm{k}\Omega$, and $T_0 = 0.4990T$. Utilizing a value of $a = 13622$ in Eq. (42), Fig. 9 compares the experimental and simulation results for the harmonic wave component of the noise spectrum induced in the bistable multivibrator by EMI with an amplitude of $V_P = 0.4\,\mathrm{V}$ and a frequency of $f = 500\,\mathrm{Hz}$. Again, a good agreement is observed between the two sets of results. To further investigate the effect of EMI on the noise spectrum induced in the bistable multivibrator, the amplitude of the AC interference signal was varied between 0.2 V and 0.9 V while the frequency was maintained at a constant $f = 500\,\mathrm{Hz}$. Fig. 10 presents the corresponding experimental and simulation results for the odd-order harmonics of the induced noise spectrum. Note that in obtaining the simulation results using Eq. (42), A_1 ranges from $5364 \sim 33006\,\mu\mathrm{A}$ while A_2 ranges from $5514 \sim 33930\,\mu\mathrm{A}$. It is observed that a good agreement is obtained between the experimental and simulation results at all values of V_p.

Table 1 compares the measured and simulated peak values of the harmonic components of the maximum noise power spectral intensity for EMI with amplitudes in the range $V_P = 0.2 \sim 0.9\,\mathrm{V}$ and a constant

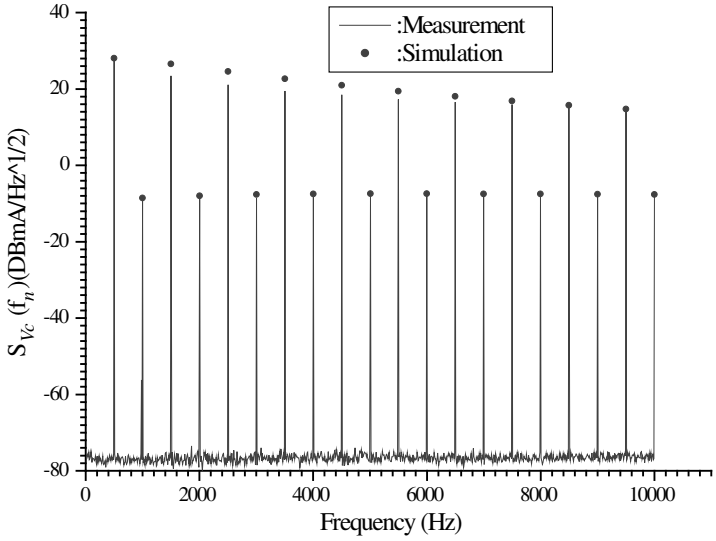

Figure 9. Harmonic wave component of bistable multivibrator noise spectrum response for $V_P = 0.4\,\mathrm{V}$ and $f = 500\,\mathrm{Hz}$. (Note that in obtaining simulation results using Eq. (42), A_1 and A_2 are specified as 12208 μA and 12549 μA, respectively.)

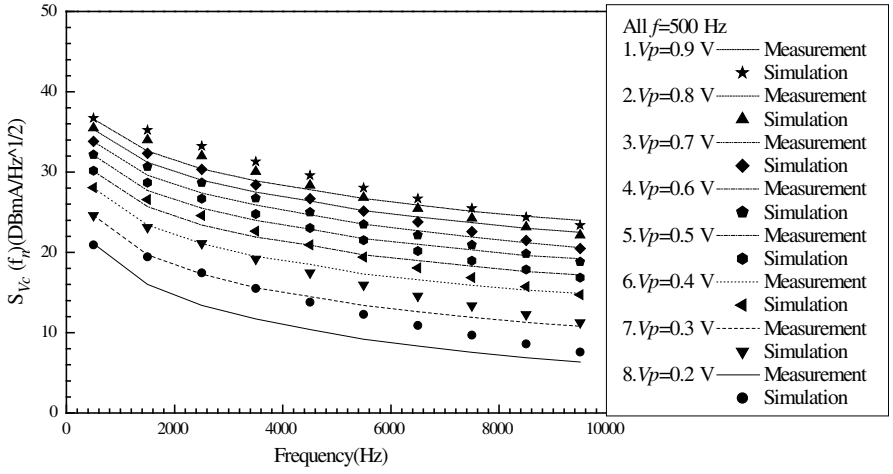

Figure 10. Experimental and simulation results for odd-order harmonics of noise spectrum induced by EMI interference with frequency of 500 Hz and amplitude of $V_p = 0.2 \sim 0.9\,\mathrm{V}$. (Simulation results computed using Eq. (42) shown using filled symbols).

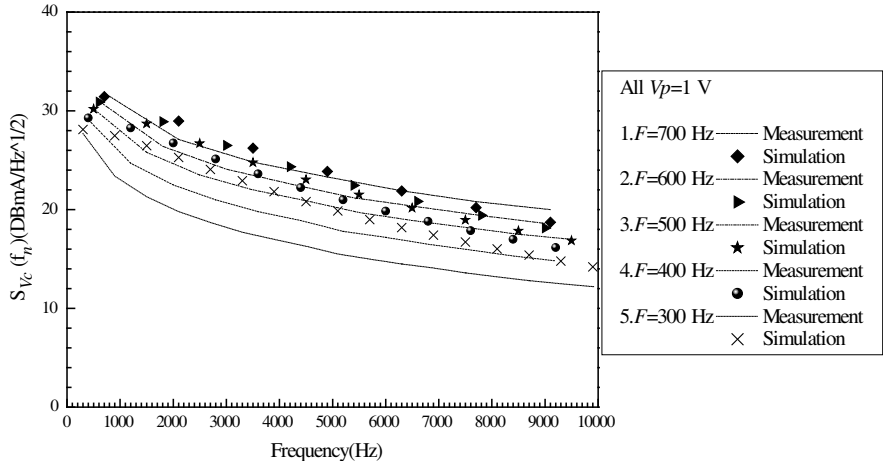

Figure 11. Experimental and simulation results for odd-order harmonics of noise spectrum induced by EMI interference frequency of $300 \sim 700\,\text{Hz}$ and amplitude of $V_p = 1\,\text{V}$. (Simulation results computed using Eq. (42) shown using filled symbols.)

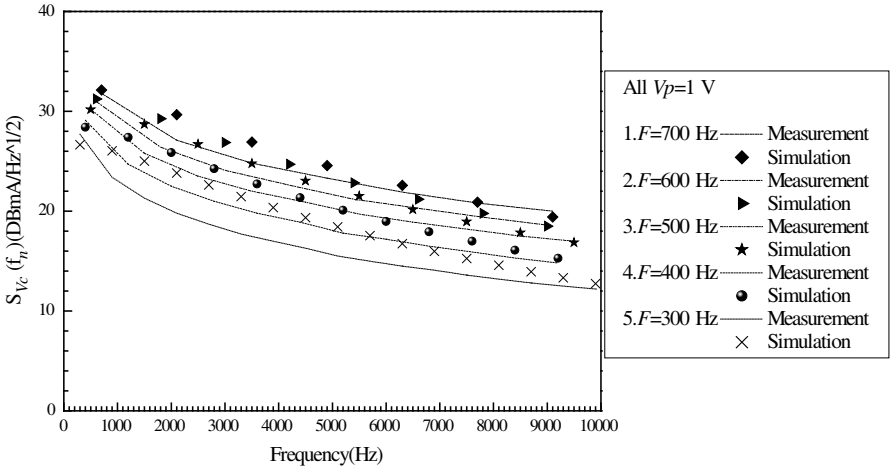

Figure 12. Experimental and simulation results for odd-order harmonics of noise spectrum induced by EMI interference frequency of $300 \sim 700\,\text{Hz}$ and variable amplitude parameters A_1 and A_2 (see Table 3). (Simulation results computed using Eq. (42) shown using filled symbols.)

Table 1. Comparison of experimental and theoretical results for maximum noise power spectral intensity for various values of V_p.

Frequency fixed, Amplitude variable (First harmonic wave)								
V_p (V)	0.2	0.3	0.4	0.5	0.6	0.7	0.8	0.9
Frequency (Hz)	500	500	500	500	500	500	500	500
Measurement (dBmA/Hz$^{1/2}$)	21.1	24.6	28	30.2	32.1	33.8	35.3	36.6
Simulation (dBmA/Hz$^{1/2}$)	20.90	24.6	28.07	30.18	32.15	33.82	35.47	36.71

Table 2. Comparison of experimental and theoretical results for maximum noise power spectral intensity for various values of frequency.

Amplitude fixed, Frequency variable (First harmonic wave)								
Frequency (Hz)	200	300	400	500	600	700	800	900
Measurement (dBmA/Hz$^{1/2}$)	25.6	27.7	29.1	30.2	31	31.8	32.3	32.7
Simulation (dBmA/Hz$^{1/2}$)	26.39	28.1	29.29	30.18	30.87	31.43	31.89	32.27

frequency of $f = 500\,\text{Hz}$, i.e., the harmonic value varies only as a function of the interference amplitude while the remaining parameters are constant. Table 2 compares the experimental and simulation results for the maximum noise power spectral intensity for EMI frequencies in the range $200 \sim 900\,\text{Hz}$ and a constant interference amplitude of $A_1 = 15565\,\mu\text{A}$ and $A_2 = 16001\,\mu\text{A}$, i.e., the noise power spectral intensity varies only as a function of the AC interference frequency while the other parameters remain constant. Fig. 11 presents the experimental and simulation results for the odd-order harmonics of the noise spectrum induced by EMI interference with a frequency of $300 \sim 700\,\text{Hz}$ and an amplitude of $V_p = 1\,\text{V}$. Although a $-2\,\text{dB}$ difference is observed between the two sets of results, it is clear that the EMI frequency has a significant effect upon the noise response of the multivibrator. By tuning the amplitude parameters in recognition of the fact that a variable EMI frequency affects both the attenuation factor and the induced wave type, the same degree of simulation accuracy as that shown in Fig. 10 can be obtained, as shown in Fig. 12 and Table 3. In other words, the EMI frequency is a function

of the EMI amplitude, as proven in Eqs. (29) and (42). Although Fig. 11 shows that the frequency has a significant effect on the odd-order harmonic waves, i.e., Eq. (42) denotes $d\omega/dA_1 \neq 0$ and $d\omega/dA_2 \neq 0$ for the nonlinear function $S_{\Delta Vc}(f_n)$, Fig. 9 shows that the difference between the experimental and simulation results for the variable amplitude case is less than that for the variable frequency case. In other words, the amplitude of the EMI has a greater effect on the noise response of the bistable multivibrator than the EMI frequency. In practice, this finding implies that the parasitic capacitance and the dynamic input resistance of the multivibrator vary with a varying frequency.

Table 3. Comparison of experimental and theoretical results for maximum noise power spectral intensity for various values of frequency and amplitude.

Amplitude, Frequency variable (First harmonic wave)					
Frequency (Hz)	300	400	500	600	700
Induced Current A_1 (μA)	13165	14065	15565	16065	16865
Induced Current A_2 (μA)	13533	14459	16001	16515	17337
Measurement (dBmA/Hz$^{1/2}$)	27.7	29.1	30.2	31	31.8
Simulation (dBmA/Hz$^{1/2}$)	26.65	28.41	30.18	31.24	32.13

Table 4. Comparison the simulations for various values of frequency, amplitude and attenuation factor with $V_p = 0.2\,\mathrm{V}$, $f = 500\,\mathrm{Hz}$.

Parameters	a	A_1 (μA)	A_2 (μA)	Remarks (Shown in)
Curve a.	13622	5364	5514	Figs. 10, 13
Curve b.	11376	4624	4753	Fig. 13
Curve c.	8622	3642	3742	Fig. 13

Table 5. Relative SNR of current induced by EMI.

V_P (V)	0.9	0.8	0.7	0.6	0.5	0.4	0.3	0.2
Induced Current A_1 (μA)	33006	28643	23661	19534	15565	12208	8193	5364
Induced Current A_2 (μA)	33930	29445	24323	20081	16001	12549	8422	5514
Induced Peak Current N_i (μA)	6.6936	5.8088	4.7984	3.9615	3.1566	2.4757	1.6615	1.0878
Relative SNR (dBμA)	3.487*	4.718*	6.378*	8.043*	10.016*	12.126*	15.590*	19.269*

*where SNR $= 20\log(S_i/N_i)$, $S_i = 10\,\mu$A, $N_i = ((A_1 + A_2)/2)/5000$ and $f = 500\,$Hz.

If we want to probe the more accuracy of Fig. 10, the attenuation factor a must be considered as a variable of power spectral intensity function. We take a curve of $V_P = 0.2\,$V in Fig. 10 to illustrate the result. Table 4 shows the noise power spectral intensity varies as a function of the AC interference frequency, amplitude and attenuation factor a, we can find that the simulation of curve b and c in Fig. 13 reveal the more accuracy than curve a. In general, the simulation and experimental results presented above indicate that the magnitude of the EMI induced by the CW is affected by the amplitude, frequency and period of the interference signal, the drain resistance and parasitic capacitance of the multivibrator, the output load, and parameter a. Table 5 indicates the relative signal-to-noise (SNR) ratio of the multivibrator for interference amplitudes in the range $V_P = 0.2 \sim 0.9\,$V, a constant frequency of $f = 500\,$Hz and a reference signal Si of $10\,\mu$A. The CW used in the present EMI experiments has a length of 1 cm. Thus, if the CW in a practical electrical circuit has a length of 1 m (say), the EMI effects will potentially be magnified 100 times compared to that observed in the present study. For example, assuming an induced current of $3.157\,\mu$A, a CW of length 1 cm, and a load resistance of $45\,\Omega$, the induced voltage is $142\,\mu$V. This value may then be amplified by up to 1000 times in a practical system, and thus a significant EMI effect occurs. According to CISPR 11 (The

International Special Committee on Radio Interference), EMI should be limited to no more than 110 dBμV in the interference frequency range $0.009 \sim 0.050$ MHz, equivalent to a voltage of 316227 μV. As a result, a useful design guideline of 2.226 cm for the maximum length of the CW in bistable multivibrator circuits can be inferred. The basic theorem presented in this paper is applicable to different circuits. However, the actual derived formulae are specific to the particular circuit. If the EMI perturbs the Wien bridge oscillator (WBO) as Fig. 14, the same results as those obtained in the present discussions. Fig. 15 compares the experimental and simulation results obtained for the harmonic components in the noise spectrum of a WBO for $V_P = 0.3\,\text{V} \sim 1.0\,\text{V}$. Comparing these results with those presented in Fig. 10 for the bistable multivibrator, it can be seen that the results are broadly similar. However, the function level is somewhat higher due to the different parameters of the two circuits.

The preceding discussions have considered the effects of low frequency interference. However, as shown in the following, the basic theorems developed in this study can also be applied to the case of high frequency interference. Fig. 16 shows that a good agreement is obtained between the experimental results and the simulation results for the noise spectrum responses induced by EMI with a frequency of 500 kHz with $V_p = 0.4 \sim 1.6\,\text{V}$ of MOSFET circuit.

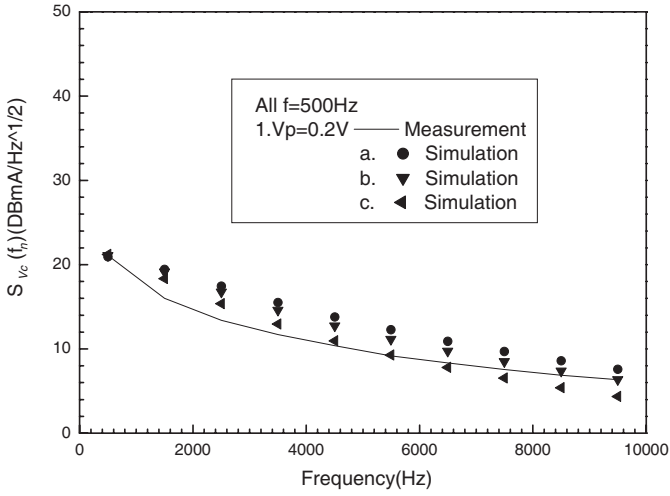

Figure 13. The noise power spectral intensity varies as a function of the AC interference frequency, amplitude and the attenuation factor a with Table 4 data.

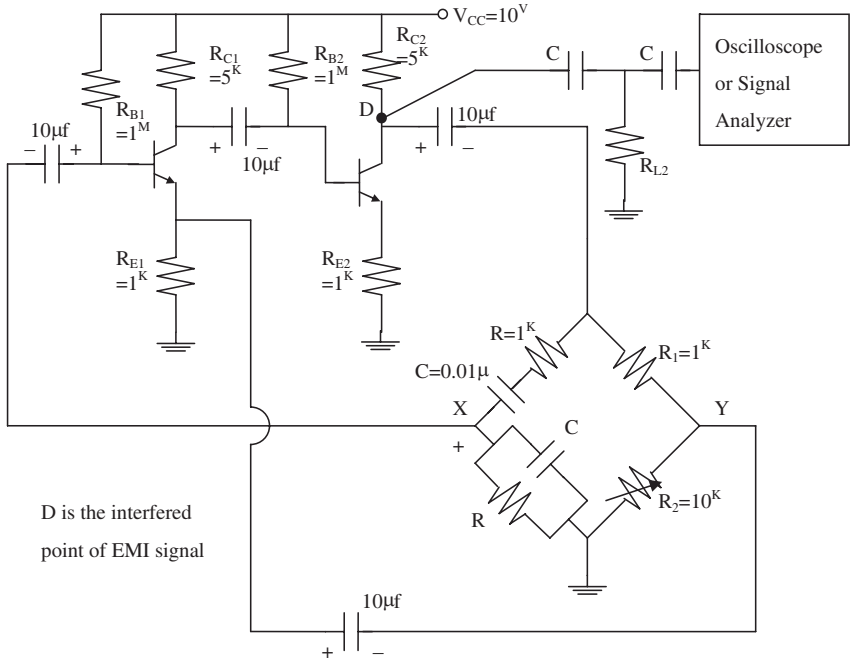

Figure 14. The circuit of WBO.

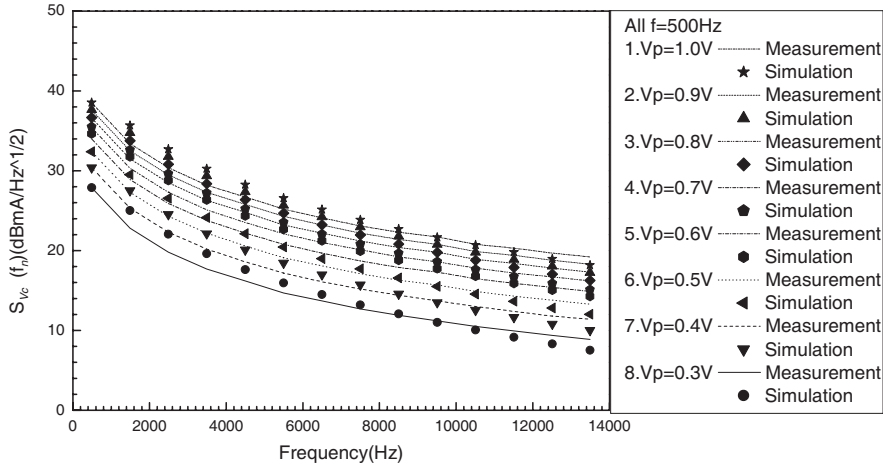

Figure 15. Experimental and simulated results for odd-order harmonics at 500 Hz with $V_p = 0.3$ V to 1.0 V of WBO.

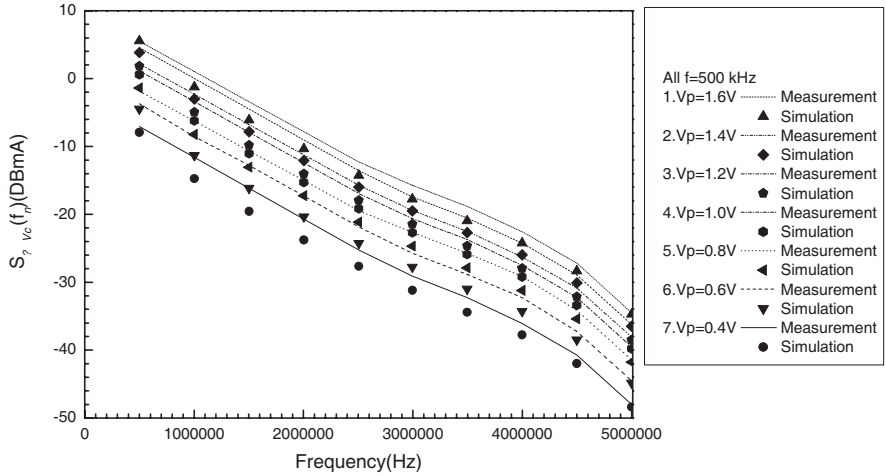

Figure 16. Experimental and simulated results at 500 kHz with $V_p = 0.4$ V to 1.6 V of MOSFET circuit.

5. CONCLUSIONS

Experimental and theoretical methods have been used to characterize the noise spectrum of a bistable multivibrator subject to periodic EMI induced via a CW. A good agreement has been observed between the experimental and simulation results for the noise spectral intensity of the bistable multivibrator in both the time domain and the frequency domain. In general, the results have shown that the noise response of the multivibrator is significantly affected by EMI. Specifically, the degree of the EMI effect on the bistable oscillator is determined by the radiated power and the following circuit parameters: f, V_0, μ_0, μ_r, N, R_ω, r_0, l_g, R_s, R_{c1}, R_{c2}, R_1, R_2, R_3, R_4, C_ω, C_{ce}, R_i, Δz, d, L, A_1, A_2, a, T_0, R_L and C. Furthermore, it has been shown that the magnitude of the induced interference current increases with an increasing interference frequency and an increasing interference amplitude. Of these two characteristics, the amplitude has a greater effect on the noise response of the multivibrator than the frequency. However, a variable EMI frequency influences both the attenuation factor and the induced wave type. In accordance with CISPR and EN norms, the results presented in this study imply that the CWs used in practical bistable multivibrator circuits should not exceed a length of 2.226 cm. Whilst the methods outlined in this study have focused specifically on the case of bistable multivibrators, they are equally applicable to the EMI analysis of all general wavelength-based electronic devices.

ACKNOWLEDGMENT

The author wishes to acknowledge the invaluable assistance provided by Haw-Jiun Liang in the course of this study.

REFERENCES

1. Masya, S., S. Takehiko, and N. Hideya, "Numerical simulation of a potassium-seeded turbulent RF inductively coupled plasma with particles," *Thin Solid Films*, Vol. 435, No. 1–2, 5–12, July 1, 2003.
2. Kwang, J. K., H. K. Jong, and H. K. Ji, "Structural and optical characterization of Cu_3N films prepared by reactive RF magnetron sputtering," *Journal of Crystal Growth*, Vol. 222, No. 4, 767–772, February, 2001.
3. Xue, J. X. and T. D. Todd, "Basestation collaboration in bluetooth voice networks," *Computer Networks*, Vol. 41, No. 3, 289–301, February 21, 2003.
4. Dai, D., "Bluetooth," *Network Security*, Vol. 2002, No. 4, 11–12, April 1, 2002.
5. Khah, S. K., T. Chakravarty, and P. Balamurali, "Analysis of an electromagnetically coupled microstrip ring antenna using an extended feedline," *Journal of Electromagnetic Waves and Applications*, Vol. 23, No. 2–3, 369–376, 2009.
6. Hong, J.-I., S.-M. Hwang, and C.-S. Huh, "Susceptibility of microcontroller devices due to coupling effects under narrow-band high power electromagnetic waves by magnetron," *Journal of Electromagnetic Waves and Applications*, Vol. 22, No. 17–18, 2451–2462, 2009.
7. Tsai, H. C. and K. C. Wang, "Investigation of EMI-induced noise spectrum on an enhancement-type MOSFET," *Solid State Electronics*, Vol. 52, No. 8, 1207–1216, 2008.
8. Kim, Y. J., U. Choi, and Y. S. Kim, "Screen filter design considerations for plasma display panels (PDP) to achieve a high brightness with a minimal loss of EMI shielding effectiveness," *Journal of Electromagnetic Waves and Applications*, Vol. 22, No. 5–6, 775–786, 2008.
9. Tsai, H. C., "Numerical and experimental analysis of EMI effects on circuits with MESFET devices," *Microelectronics Reliability*, Vol. 48, No. 4, 537–546, 2008.
10. Wessels, P., M. van Swanenberg, H. Zwol, B. Krabbenborg, H. Boezen, M. Berkhout, et al., "Advanced BCD technology

for automotive, audio and power applications," *Solid State Electronics*, Vol. 51, No. 2, 195–211, 2007.

11. Tsai, H. C., "An investigation on the influence of electromagnetic interference induced in conducting wire of universal LEDs," *Microelectronics Reliability*, Vol. 47, No. 6, 959–966, 2007.
12. Tsai, H. C., "An investigation into EMI-induced noise in nanometer multi-quantum well InGaN LEDs," *Optics Communications*, Vol. 273, No. 2, 311–319, 2007.
13. Michette, A. G., S. J. Pfauntsch, A. Erko, A. Firsov, and A. Svintsov, "Nanometer focusing of X-rays with modified reflection zone plates," *Optics Communications*, Vol. 245, No. 1–6, 249–253, 2005.
14. Busatto, G., L. Fratelli, C. Abbate, R. Mamzo, and F. Iannuzzo, "Analysis and optimisation through innovative driving strategy of high power IGBT performances/EMI reduction trade-off for converter systems in railway applications," *Microelectronics Reliability*, Vol. 44, No. 9–11, 1443–1448, 2004.
15. Quach, H. P. and C. P. Chui Talso, "Low temperature magnetic properties of Metglas 2714A and its potential use as core material for EMI filters," *Cryogenics*, Vol. 44, No. 6–8, 445–449, 2004.
16. Steinecke, T., H. Koehne, and M. Schmidt, "Behavioral EMI models of complex digital VLSI circuits," *Microelectronics Journal*, Vol. 35, No. 6, 547–555, 2004.
17. Vasa, P., B. P. Singh, P. Taneja, and P. Ayyub, "Antiresonant ring interferometry as a sensitive technique for measuring nonlinear optical properties of thin films," *Optics Communications*, Vol. 233, No. 1–6, 297–304, 2004.
18. Tsai, H. C., "Reliable study of digital IC circuits with margin voltage among variable DC power supply, electromagnetic interference and conducting wire antenna," *Microelectronics Reliability*, Vol. 43, No. 12, 2001–2009, 2003.
19. Tsai, H. C., "Impact of electromagnetic radiation induced by conducting wire antenna on optical fiber communication systems," *Optics Communications*, Vol. 223, No. 1–3, 81–89, 2003.
20. Lee, T.-H. and H.-D. Kim, "Radiation hardness test of preamplifier circuits composed of commercial bipolar transistors," *Nuclear Inst. and Methods in Physics Research, A*, Vol. 579, No. 1, 260–263, 2007.
21. Zhao, Z., Y. M. Li, J. Cheng, and Y. F. Xu, "Current sensor utilizing giant magneto-impedance effect in amorphous ribbon toroidal core and CMOS inverter multivibrator," *Sensors &*

Actuators: A. Physical, Vol. 137, No. 1, 64–67, 2007.

22. Muselli, M., "Frequency analysis of binary oscillators triggered by a random noise," *Physica D*, Vol. 188, No. 1–2, 119–133, 2004.
23. Cheng, D. K., *Field and Wave Electromagnetics*, 2nd edition, 252–634, Addison-Wesley Publishing Company, USA, 1989.
24. Bhatia, V. and B. Mulgrew, "Non-parametric likelihood based channel estimator for Gaussian mixture noise," *Signal Processing*, Vol. 87, No. 11, 2569–2586, 2007.
25. Chambers, J., D. Bullock, Y. Kahana, A. Kots, and A. Palmer, "Developments in active noise control sound systems for magnetic resonance imaging," *Applied Acoustics*, Vol. 68, No. 3, 281–295, 2007.
26. Yuan, J., "Adaptive Laguerre filters for active noise control," *Applied Acoustics*, Vol. 68, No. 1, 86–96, 2007.
27. Roelant, R., D. Constales, G. S. Yablonsky, R. Van Keer, M. A. Rude, and G. B. Marin, "Noise in temporal analysis of products (TAP) pulse responses," *Catalysis Today*, Vol. 121, No. 3–4, 269–281, 2007.
28. Lisnanski, R. and A. J. Weiss, "Low complexity generalized EM algorithm for blind channel estimation and data detection in optical communication systems," *Signal Processing*, Vol. 86, No. 11, 3393–3403, 2006.
29. Li, H. G. and G. Meng, "Detection of harmonic signals from chaotic interference by empirical mode decomposition," *Chaos, Solitons and Fractals*, Vol. 30, No. 4, 930–935, 2006.
30. Van Der Ziel, A., *Noise in Solid State Devices and Circuits*, 10–20, Wiley, New York, 1986.